Phase transformation and morphology tuning of β-$NaYF_4$:Yb^{3+},Er^{3+} nanocrystals through K^+ ions codoping*

Liang Zhi-Qin(梁志琴)[a)b)], Zhao Su-Ling(赵谡玲)[a)b)†], Cui Yue(崔 越)[a)b)], Tian Li-Jiao(田丽娇)[a)b)], Zhang Jun-Jie(张俊杰)[a)b)], and Xu Zheng(徐 征)[a)b)]

[a)] *Key Laboratory of Luminescence and Optical Information, Beijing Jiaotong University, Ministry of Education, Beijing* 100044, *China*
[b)] *Institute of Optoelectronics Technology, Beijing Jiaotong University, Beijing* 100044, *China*

(Received 28 July 2014; revised manuscript received 16 October 2014; published online 19 January 2015)

In this work, a simple method to modulate the crystal phase and morphology with a large amount of K^+ ions codoping is proposed. The phase changes to the mixture of β-$NaYF_4$ and β-KYF_4 with increasing the content of K^+ ions to 80 mol%. When it exceeds 80 mol%, β-$NaYF_4$ disappears gradually and β-KYF_4 dominates with a poor crystalline. In addition, the morphology changes from nanosphere to nanoplate, and then to nanoprism, which indicates that a higher content of K^+ ions favors the growth rates along [0001] than the [10-10] of the nanocrystals. Additionally, the upconversion (UC) luminescence properties and the ratio of red/green (R/G) UC intensity of samples with different phases and morphologies are detected, which makes it possible to tune the UC fluorescence by varying the concentration of K^+ ions.

Keywords: upconversion fluorescence, $NaYF_4$:Yb,Er, K^+ ions codoping

PACS: 78.40.−q, 74.25.Gz, 42.70.−a, 78.67.Bf **DOI:** 10.1088/1674-1056/24/3/037801

1. Introduction

Rare-earth ions doped inorganic materials are a kind of upconversion fluorescence materials which have a great application prospect in many fields, such as three-dimensional (3D) display,[1] UC lasers,[2] bioimaging,[3,4] therapy,[5] and optical memory[6] due to their unique advantages compared with traditional organic dyes and semiconductor quantum dots, including weak autofluorescence backgrounds, deep penetration abilities, resistance to photobleaching and low toxicity, *et al.*[7,8] Among all of these materials, Yb, Er (or Yb, Tm) co-doped fluorides have been reported to be the most efficient upconversion material for green (or blue) emission due to their low phonon energy (~ 350 cm^{-1}), low non-radiative probability, and this accordingly increases the luminescence intensity.[9–11]

Nowadays, the manipulation of upconversion (UC) nanocrystals with controllable morphologies and sizes remains the research focus because of their great potential in improving the emission intensity, changing emission ratios, and tuning the multi-color luminescence.[12] So far, many efforts have been dedicated to preparing nanocrystals with multiple morphologies and phases.[13–16] Traditional methods to achieve phase transformation and morphology tuning usually manipulate several experimental parameters, such as reactant concentration, reaction time, and reaction temperature.[17,21] The problems faced by these methods mainly concentrate on the higher demand for the reaction conditions and the difficulty in tuning the size over a broad range.

More recently, impurity doping has emerged as an important route to easily change the morphology and phase, which requires only a change of the dopant concentration, whereas it provides tremendous improvements in the control of the phase and morphology. K element is from the same alkali group as Na element, which makes it possible to replace Na with K and this accordingly achieves the precisely architectural manipulation with well-defined morphologies and phases. In fact, in recent years there have been some researches on K^+ ions codoping in β-$NaYF_4$ matrix. Typically, Zhao's group[22] reported that the morphology kept microrods, although it increased K^+ ions to 85 mol%, that is, almost no morphology changes in this process. Zhang's group[23] and Vishal Kal's group[24] presented the crystal structure and UC emission spectra by K^+ ions codoping. However, there is still lack of a systematic study of how the phase and morphology change regularly when the content of K^+ ions increases gradually.

Herein, as the focus of this article, we discuss how a regular control over the crystal phases and morphologies of the nanocrystals can be achieved by simply varying the codoped concentration of K^+ ions. In addition, we also measure the UC luminescence of the samples with different phases and morphologies.

2. Experimental section

The rare earth chlorides $RECl_3$ (YCl_3, $YbCl_3$, and $ErCl_3$, 99.99%), oleic acid (OA, 90%), 1-octadecene (ODE,

*Project supported by the National High Technology Research and Development Program of China (Grant No. 2013AA032205), the National Natural Science Foundation of China (Grant No. 51272022), and the Fundamental Research Funds for the Central Universities, China (Grant No. 2012JBZ001).

†Corresponding author. E-mail: slzhao@bjtu.edu.cn

© 2015 Chinese Physical Society and IOP Publishing Ltd

90%), ammonium fluoride (NH_4F, $\geq 98\%$), sodium hydroxide (NaOH, 99.99%), potassium hydroxide (KOH, 99.99%), absolute methanol ($\geq 99.9\%$) and cyclohexane ($\geq 99.5\%$) were purchased from Sigma-Aldrich. All of the chemicals were used directly without any further purification.

For a typical synthesis of β-Na(K)YF_4:Yb^{3+},Er^{3+} nanocrystals similar to the procedure reported previously,[25] 1-mmol YCl_3, $YbCl_3$, and $ErCl_3$ in a ratio of 78:20:2 were added into a 50-ml flask containing 6 ml of OA and 15 ml of ODE. The solution was heated to 160 °C for 20 min and then cooled down to room temperature. Subsequently, 10-ml methanol solution containing a total of 2.5-mmol NaOH and KOH with corresponding molar ratios and 4-mmol NH_4F were added into the flask dropwise, which was stirred for 30 min to ensure that all of the fluoride has been completely consumed. After the methanol was evaporated, the solution was heated to 300 °C and maintained for 1.5 h. The whole process was protected in an argon environment. The resulting nanocrystals were precipitated by ethanol and washed with ethanol and water several times and then dried at 50 °C overnight.

Powder x-ray diffraction (XRD) patterns of the samples were performed with a x-ray diffractometer with Cu Kα_1 radiation ($\lambda = 1.540$ Å). The morphology and size of the synthesized nanocrystals were characterized by transmission electron microscopy (TEM) using a JEOL-2100F TEM. Scaning electron microscope (SEM) measurements were performed using a Hitachi, S-4800 SEM equipped with the energy dispersive x-ray (EDX) spectrum. UC emission spectra were collected using a 980-nm diode laser (BWT Beijing LTD) as the excitation source and detected by SPEX Fluordlog-3 Fluorescence Spectrometer from 350–700 nm. All of these measurements were performed at room temperature.

3. Results and discussion

Figure 1 shows the XRD patterns of all as-prepared samples after codoping with x mol% K^+ ions ($x = 0$, 20, 40, 60, 80, 100), respectively. The crystal structure is dominated by the hexagonal $NaYF_4$ until the content of K^+ ions exceeds 60 mol%. When the concentration of K^+ ions reaches 80 mol%, there are more β-KYF_4 nanoparticles formed and β-$NaYF_4$ nanocrystals are no longer dominated. In case of 100 mol% K^+ ions, the hexagonal $NaYF_4$ phase disappears and the poor crystalline KYF_4 totally exists in the phase. Obviously, the phase transformation from $NaYF_4$ to KYF_4 is closely related to the amount of K^+ ions codoping. When there are not enough codoped K^+ ions to form β-KYF_4 hexagonal $NaYF_4$ dominates with a good crystalline. Thereafter, a relatively large amount of K^+ ions are doped into the crystal, the imbalance of the intrinsic structure caused by K^+ ions plays a role due to K^+ ions occupy only the substitution positions of Na^+ ions, then β-KYF_4 appears. When the remaining Na^+ ions are too few to any longer form a stable $NaYF_4$ phase, the KYF_4 dominates with poor crystalline.

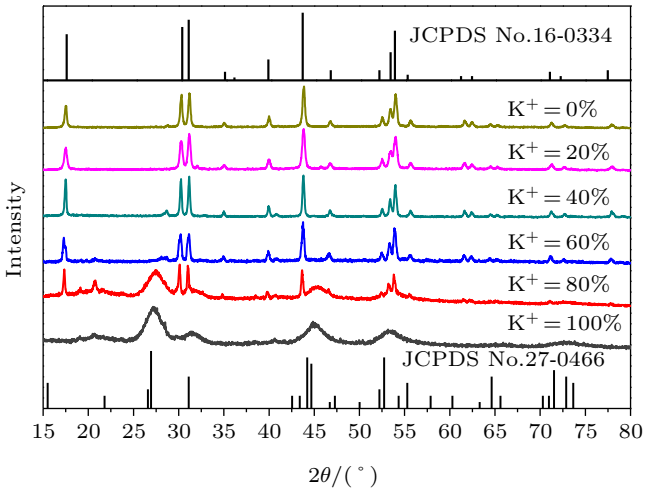


Fig. 1. (color online) XRD patterns of the nanocrystals codoped with different contents of K^+ ions and the standard data of β-$NaYF_4$ (JCPDS No. 16-0334) and β-KYF_4 (JCPDS No. 27-0466).

The effect of the amount of K^+ ions on the morphology and size has been investigated by TEM, as shown in Fig. 2. Spherical nanoparticles with an average diameter of about 26 nm are obtained when there is no K^+ introduced (Fig. 2(a)). As the content of K^+ ions increase to 20 mol%, most of the nanocrystals are uniform in size with a regular hexagonal cross-section (Fig. 2(b)). As the codoped K^+ ions continually increase to 40 mol%, the shape turns into a rectangular-like cross-section with uneven top-bottom surface (Fig. 2(c)) and, subsequently, it remarkably becomes longer along the cross-section with a further increase in K^+ ions content to 80 mol% (Figs. 2(d) and 2(e)). For the amount of 80–100 mol% K^+ ions, the spherical hexagonal KYF_4 dominates with almost 20 nm (Fig. 2(f)). The inset in Fig. 2(f) presents a typical HRTEM image of β-KYF_4 nanocrystals, and it reveals that the as-obtained β-KYF_4 nanocrystals are a single crystalline with clear lattice fringes with an interplaner spacing of 0.469 nm, which coincides with the lattice spacing for (012) planes of the β-KYF_4 conforming the formation of β-KYF_4 nanocrystals.

The SEM images present in Fig. 3 can provide further insight into the morphology changes with different codoping content of K^+ ions. The regular hexagonal plate-like can be observed with 20 mol% K^+ ions (Fig. 3(a)), the shape then changes from nanoplate to nanoprism as the content of K^+ ions further increases. These phase transformations from SEM images are consistent with the results shown in the TEM images. The energy dispersive x-ray spectroscopy (EDX) results (Figs. 3(b), 3(e), and 3(h)) reveal that the samples are mainly composed of Na, K, Y, Yb, Er, which coincide with the initial elements.

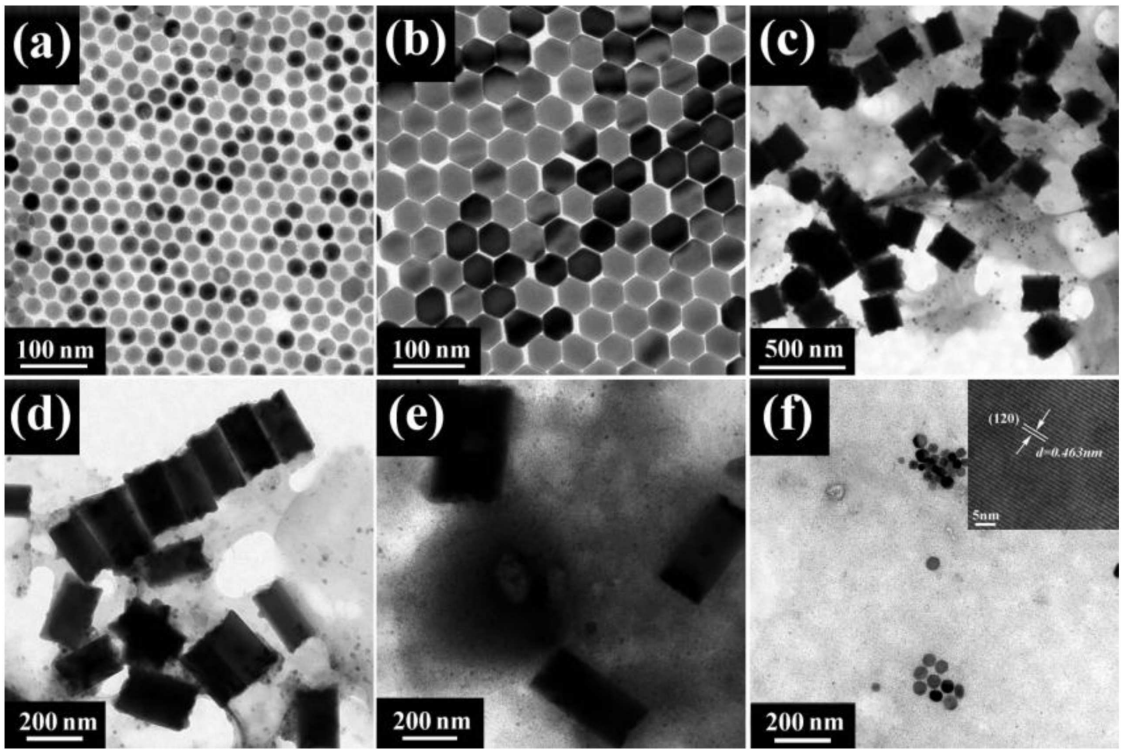


Fig. 2. TEM images of the as-precipitated nanocrystals: (a) $K^+ = 0$ mol%, (b) $K^+ = 20$ mol%, (c) $K^+ = 40$ mol%, (d) $K^+ = 60$ mol%, (e) $K^+ = 80$ mol%, (f) $K^+ = 100$ mol%. The inset in panel (f) shows the HRTEM images of the products in panel (f).

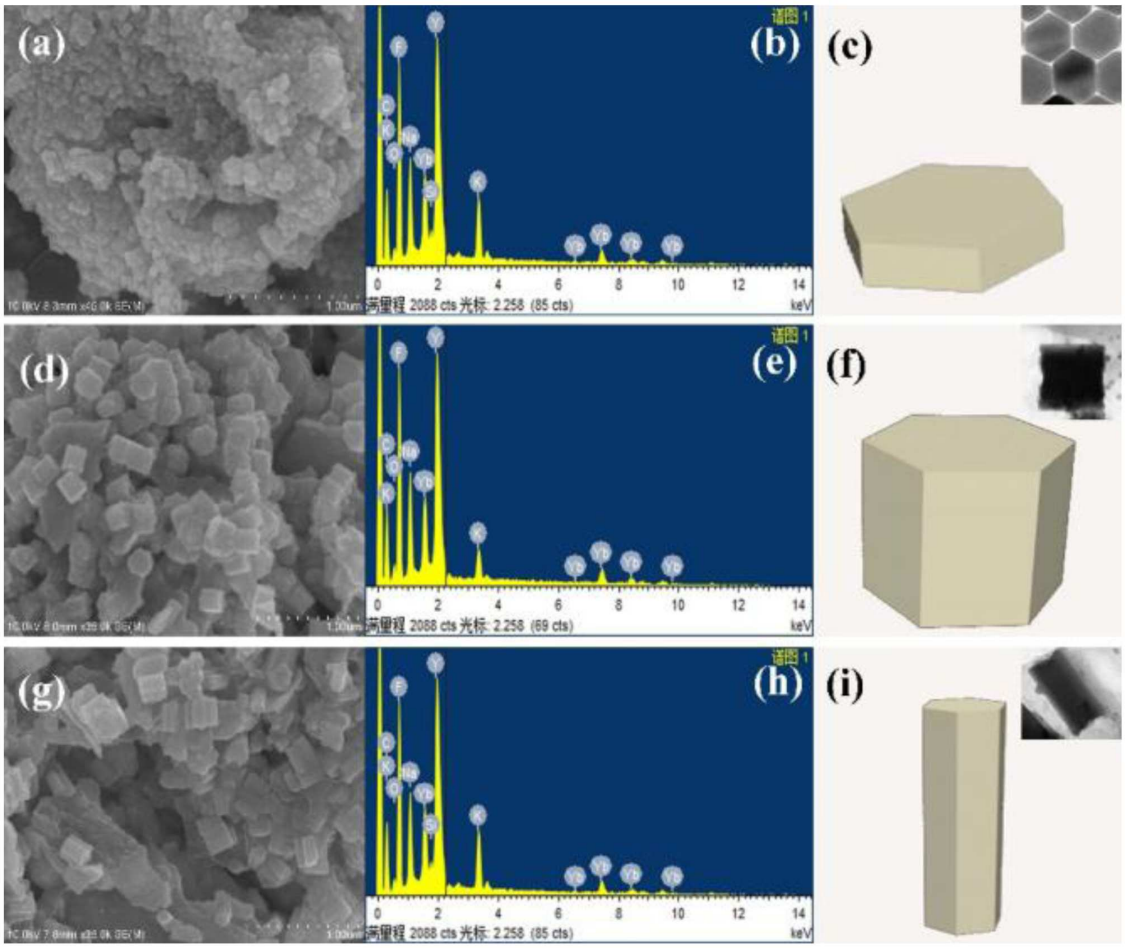


Fig. 3. (color online) SEM, EDX images, and schematic structures: (a)–(c) 20 mol% K^+ ions, (d)–(f) 40 mol% K^+ ions, and (g)–(i) 60 mol% K^+ ions.

The schematic structures (Figs. 3(c), 3(f), and 3(i)) concretely display the morphology changes. As is well known, the surfaces of hexagonal nanoprisms consist of {0001} top/bottom planes and six energetically equivalent {10-10} families of prismatic side planes.[26] The anisotropic structures of the thermodynamically stable hexagonal $NaYF_4$ nanoparticles induce anisotropic growth along their crystallographically reactive directions, which results in anisotropic shapes of the nanocrystals.[27] According to the Gibbs–Thompson theory, the relative chemical potential of a crystal is proportional to its surface-atom ratio, which is determined by the average number of dangling bonds per atom over the whole crystal.[28] The capping effect of F^- can decrease the average number of dangling bonds and further decrease the chemical potential of the crystal.[29] With an increase in the content of K^+ ions, the amount of Na^+ ions combined with F^- gradually decreases, while the amount of Y^{3+} ions keeps constant. Detailed observation on the crystal structure of β-$NaYF_4$ revealed that the density of Y^{3+} on the {10-10} is higher than that on the {0001} planes. Therefore, there are more Y^{3+} ions attaching to the six equivalent {10-10} faces when more Na^+ ions are replaced by K^+ ions, which results in the capping effect of F^- on the {10-10} plane being greater than on the {0001} plane. So the chemical potential of {10-10} plane decreases while that of the {0001} plane increases accordingly. Consequently, the growth rate of the nanocrystals along the {0001} is much quicker than that along the {10-10} , therefore the morphologies from nanoplate to nanoprism, and then to nanorod have been produced. In addition, fast growth on the edges rather than in the center leads to an uneven top-bottom surface.

The UC luminescence spectra of the synthesized nanoparticles were measured at room temperature under 980-nm excitation, as shown in Fig. 4(a). For all of the samples, the sample with 20 mol% K^+ ions shows the maximum UC luminescence intensity in comparison with the others under the same condition. Thereafter, the UC intensity starts to decrease with further increase of the content of K^+ ions. Such an enhancement in UC luminescence intensity may be caused by two factors. One is that the local crystal field could be tailored when introducing K^+ ions into the $NaYF_4$ matrix, which may decrease the intrinsic symmetry around Er^{3+} ions. According to previous reports,[32,33] lower crystals field symmetry will lead to an increase in the electric dipole transition probability and thereby enhances the UC intensity. But with more K^+ ions codoped into the host materials, the symmetry around the environment of Er^{3+} ions is gradually better, giving rise to the decreased UC emission intensity. In this work, when the concentration of K^+ ions equals to 20 mol%, the crystal field symmetry is the lowest, therefore 20 mol% K^+ ions shows the maximum UC intensity. The other factor is that the distance between Yb^{3+}- and Er^{3+} ions changes when introducing a large amount of K^+ ions. In the starting materials, the Na/R ratio decreases in the $NaYF_4$ lattice as the content of K^+ ions increases to 20 mol%. This may decreases the distance between Yb^{3+} and Er^{3+} ions, which contributes to the easy energy transfer. However, with a further increase of K^+ ions to 40 mol%, the close distance between rare-earth ions, which is too close, results in the concentration quenching, which decreases the UC emission intensity.

It is worth noting that such a comparison of emission intensity does not make much sense, although the samples present different UC emission[32] because the phase and morphology change a lot after codoping with different concentrations of K^+ ions, which affects the scattering and absorption of incident light. In addition, the number of luminescence centers is related to the size of the nanocrystals. However, it is difficult to satisfy the same luminescence center. When the intensity is normalized according to the green emission peak at 541 nm, the value of I_{red}/I_{green} decreases as the amount of K^+ ions increases, as shown in Fig. 4(b). This may be attributed to the fact that more electrons go to the splitting $^4I_{11/2}$ of Er^{3+} caused by the changed crystal lattice with K^+ ions codoped, leading to an increased chance that the electrons on this level are further excited to the $^4F_{7/2}$, and at last an enhanced green emission.[23]

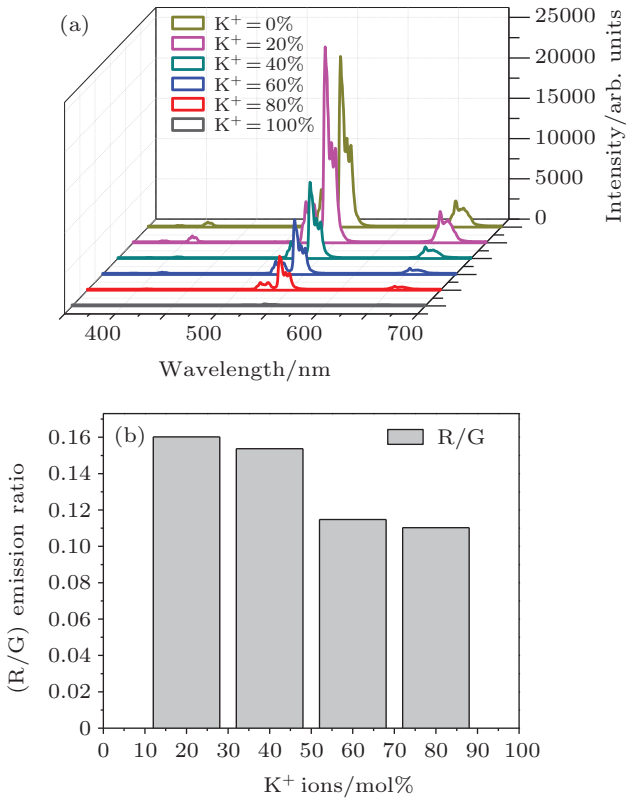


Fig. 4. (color online) (a) UC emission spectra of the samples with different concentrations of K^+ ions. All of them are measured under the same conditions. (b) Red-to green (R/G) emission ratios as a function of the content of K^+ ions.

The UC luminescence intensities were measured as a function of the pump power for β-$NaYF_4$:Yb^{3+},Er^{3+} and β-

KYF_4:Yb^{3+},Er^{3+} nanocrystals in order to determine the number of photons responsible for the UC mechanism.[34] For an unsaturated UC process, the emission intensity (I) is proportional to the excitation power (P): $I = P^n$, in which n is the number of pump photons required.[31] As shown in Fig. 5, the slopes n are 1.79 and 1.81 for the green and red emissions, respectively, for the $NaYF_4$:Yb^{3+},Er^{3+} nanocrystals. Likewise, for the KYF_4:Yb^{3+},Er^{3+} nanocrystals, the values n are 1.65 and 1.85 for the green and red emissions, respectively. This means that the green and red emissions for both of the samples are two-photon processes.

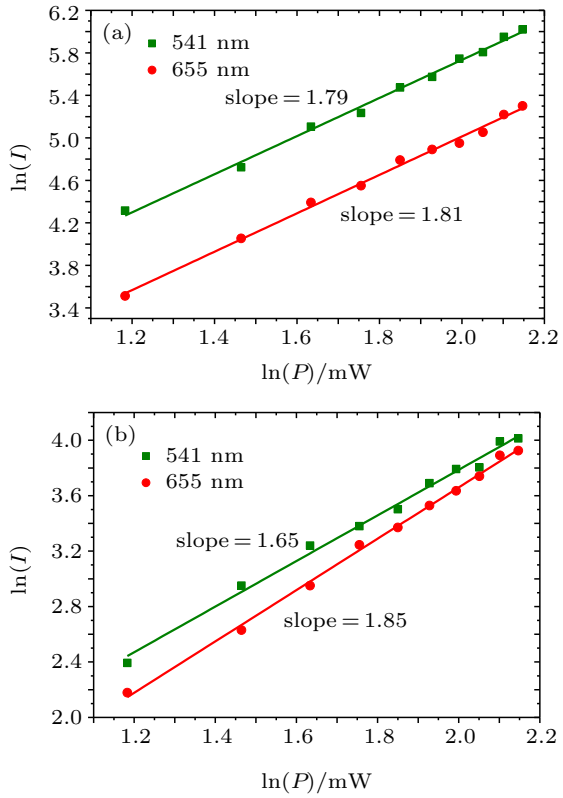


Fig. 5. (color online) Pump power dependence of the green and red emissions of (a) $NaYF_4$:Yb^{3+},Er^{3+}, (b) KYF_4:Yb^{3+},Er^{3+} nanocrystals.

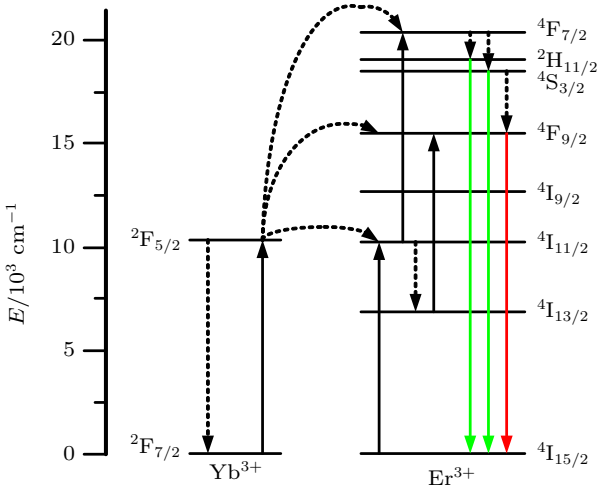


Fig. 6. (color online) A schematic diagram of UC process under 980-nm excitation.

Combined with the schematic diagram of UC process in Fig. 6, we can deduce the UC mechanism easily. In short, two successive energy transfers from Yb^{3+} ions can excite Er^{3+} ions to the $^4F_{7/2}$ level, then the Er^{3+} ions relax to the $^2H_{11/2}$ and $^4S_{3/2}$ levels due to the non-radiative process, followed with the green emission. The red emission of the $^4F_{9/2}$ level can also be populated either from the upper $^2H_{11/2}$ and $^4S_{3/2}$ level by non-radiative process, or through the non-radiative relaxtion from $^4I_{11/2}$ to $^4I_{13/2}$, then the $^4I_{13/2}$ level of Er^{3+} ions absorb an energy from excited Yb^{3+} ions, and are thereby excited to the $^4F_{9/2}$ level.[35]

4. Conclusions

In summary, we have successfully synthesized K^+ ions codoped β-$NaYF_4$:Yb^{3+},Er^{3+} nanocrystals. Systematic manipulation of the phase and morphology has been achieved by simply tuning the content of K^+ ions. It turns out that a higher content of K^+ ions favors the growth rates along [0001] than the [10-10] of β-$NaYF_4$:Yb^{3+}, Er^{3+} nanocrystals, which results in the morphology tuning from nanosphere to nanoplate, and then to nanoprism and the phase transformation from β-$NaYF_4$ to β-KYF_4. Additionally, the samples present a strong green emission under 980-nm excitation. This is a facile strategy to tuning the phase and morphology, which is helpful for further crystal-design and morphology-controlled synthesis of other nanocrystals.[36] Moreover, these obtained products present different emission spectra, which makes it possible to tune the UC fluorescence of the nanocrystals. The emission spectra tuning will enable these UC nanomaterials to offer promising application prospects in many fields, such as 3D displays, solar cells, and multiplexing bioassays.

References

[1] Wang F, Han Y, Lim C S, Li Y H, Wang J, Xu J, Chen H Y, Zhang C, Hong M H and Liu X G 2010 *Nature* **463** 1061
[2] Zhang X M, Zhang J H, Zhang X, Chen L, Lu S Z and Wang X J 2007 *J. Lumin.* **122** 958
[3] Heer S, Kömpe K, Güdel H U and Haase M 2004 *Adv. Mater.* **16** 2102
[4] Hilderbrand S A, Shao F, Salthouse C, Mahmood U and Weissleder R 2009 *Chem. Commun.* **28** 4188
[5] Idris N M, Gnanasammandhan M K, Zhang J, Ho P C, Mahendran R and Zhang Y 2012 *Nat. Med.* **18** 1580
[6] Carling C J, Boyer J C and Branda N R 2009 *J. Am. Chem. Soc.* **131** 10838
[7] Auzel F 2004 *Chem. Rev.* **104** 139
[8] Haase M and Schäfer H 2011 *Angew. Chem. Int. Ed.* **50** 5808
[9] Wang F, Deng R R, Wang J, Wang Q X, Han Y, Zhu H M, Chen X Y and Liu X G 2011 *Nat. Mater.* **10** 968
[10] Pang M, Feng J, Song S Y, Wang Z and Zhang H J 2013 *Cryst. Eng. Commun.* **15** 6901
[11] Zhang J J, Dai S X, Hu L L, Duan Z C and He D B 2006 *Chin. Phys.* **15** 209
[12] Zhao L C, Guo F Y, Li M C and Lü Q 2009 *Chin. Phys. B* **18** 4030
[13] Yang J, Li C X, Cheng Z Y, Zhang X M, Quan Z W, Zhang C M and Lin J 2007 *J. Phys. Chem. C* **111** 18148
[14] Zhang C and Chen J 2010 *Chem. Commun.* **46** 592
[15] Zeng Q H, Xue B, Zhang Y L, Wang D, Liu X M, Tu L P, Zhao H F, Kong X G and Zhang H 2013 *Cryst. Eng. Commun.* **15** 4765

[16] Ye X C, Collins J E, Kang Y J, Chen J, Chen D T N, Yodh A G and Murray C B 2010 *Proc. Nat. Acad Sci.* **107** 22430
[17] Mai H X, Zhang Y W, Si R, Yan Z G, Sun L D, You L P and Yan C H 2006 *J. Am. Chem. Soc.* **128** 6426
[18] Ahmad S, Prakash G V and Nagarajan R 2012 *Inorg. Chem.* **51** 12748
[19] Li L, Zhou Z X, Yang W L, Li H and W Y 2013 *Chin. Phys. Lett.* **30** 127103
[20] Schäfer H, Ptacek P, Eickmeier H and Haase M 2009 *Adv. Funct. Mater.* **19** 3091
[21] Lü Q, Zhao L C, Guo F Y and Li M C 2009 *Chin. Phys. B* **18** 4030
[22] Mao C S, Yang X H and Zhao L J 2013 *Chem. Eng. J.* **229** 429
[23] Dou Q Q and Zhang Y 2011 *Langmuir* **27** 13236
[24] Kale V, Soukka T, Hölsä J and Lastusaari M 2013 *J. Nanopart. Res.* **5** 1
[25] Li Z Q and Zhang Y 2008 *Nanotechnology* **19** 345606
[26] Li C X, Quan Z W, Yang J, Yang P P and Lin J 2007 *Inorg. Chem.* **46** 6329
[27] Li C X, Yang J, Quan Z W, Yang P P, Kong D Y and Lin J 2007 *Chem. Mater.* **19** 4933
[28] Liang X, Wang X, Zhuang J, Peng Q and Li Y 2007 *Adv. Funct. Mater.* **17** 2757
[29] Ding M Y, Lu C H, Cao L H, Ni Y and Xu Z Z 2013 *Cryst. Eng. Commun.* **15** 8366
[30] Patra A, Friend C S, Kapoor R and Prasad P N 2003 *Appl. Phys. Lett.* **83** 284
[31] Judd B 1962 *Phys. Rev.* **127** 750
[32] Li C X, Quan Z W, Yang P P, Huang S S, Lian H Z and Lin J 2008 *J. Phys. Chem. C* **112** 13395
[33] Liu Y X, Wang D S, Shi J X, Peng Q and Li Y D 2013 *Angew. Chem. Int. Ed.* **52** 4366
[34] Auzel F E 1973 *Proceedings of the IEEE* **61** 758
[35] Vetrone F, Boyer J C, Capobianco J A, Speghini A and Bettinelli M 2003 *Chem. Mater.* **15** 2737
[36] He E J, Liu N, Zhang M L, Qin Y F, Guan B G, Li Y and Guo M L 2012 *Chin. Phys. B* **21** 073201